Probing the sign of the Hubbard interaction by two-particle quantum walks

Andrea Beggi, Luca Razzoli, and Paolo Bordone*
Dipartimento di Scienze Fisiche, Informatiche e Matematiche, Università di Modena e Reggio Emilia, I-41125, Modena, Italy and Centro S3, CNR-Istituto di Nanoscienze, I-41125, Modena, Italy

Matteo G. A. Paris
Quantum Technology Lab, Dipartimento di Fisica dell'Università degli Studi di Milano, I-20133 Milano, Italy and INFN, Sezione di Milano, I-20133 Milano, Italy

(Received 2 November 2017; published 12 January 2018)

We address the discrimination between attractive and repulsive interaction in systems made of two identical bosons propagating on a one-dimensional lattice, and suggest a probing scheme exploiting the dynamical properties of the corresponding two-particle quantum walks. In particular, we show that the sign of the interaction leaves a clear signature in the dynamics of the two walkers, which is governed by the Hubbard model, and in their quantum correlations, thus permitting one to discriminate between the two cases. We also prove that these features are strictly connected to the band structure of the Hubbard Hamiltonian.

DOI: 10.1103/PhysRevA.97.013610

I. INTRODUCTION

The Hubbard model (HM) [1–3] well describes, in simple and general terms, the physics of several systems of correlated particles, either fermions or bosons [4], e.g., Mott insulators, ultracold atomic lattices [5–8], spin chains [9,10], and nonlinear waveguides [11–15]. In the limit of large interactions, the HM may be mapped onto the XXZ Heisenberg model [9,16] and may be employed to describe the propagation of interacting identical particles [17–19] on one-dimensional lattice, where the interaction can be either attractive or repulsive, depending on the chosen physical implementation. Remarkably, there are systems where both possibilities are contemplated [12,20–22].

Recent experimental results on cold atoms in an optical lattice showed that a bounded pair of interacting particles can be formed even under the action of a repulsive potential [5,21,23–25]. This phenomenon has a clear physical explanation by looking at the band structure of the model, which behaves symmetrically under the exchange of sign in the interaction term: for both attractive and repulsive potentials, the onset of the interaction creates a separate *miniband* hosting bounded states, thus determining the copropagation of the particles that are initially placed on the same site [11,26]. This remarkable result has suggested that the behavior of the model is fully symmetrical under the exchange of sign of the interaction, and some following works [11] pointed out that there are no differences in the correlations among particles when the interaction potential switches from positive to negative values.

On the other hand, some recent studies about the Hubbard dynamics of identical particles [14,27,28] have shown that for some specific initial states, the HM may lead to different dynamics for attractive and repulsive interactions. These features are remarkable and may be of interest for applications, since they could be exploited to engineer entanglement among particles at a deeper level, granting us a further degree of freedom to perform (quantum) computational tasks.

Motivated by these results, we address here the discrimination between attractive and repulsive interaction for two identical bosons propagating on a one-dimensional lattice according to the Hubbard model. In particular, we show that the sign of the interaction clearly influences the evolution of the system, as well as the nature of the particle correlations, thus permitting distinction between the two cases. We also devote attention to prove that these features are intimately connected to the band structure of the Hubbard Hamiltonian.

Our probing scheme is based on the fact that the Hubbard Hamiltonian is well suited to describe the quantum walks of identical particles on a one-dimensional lattice. In turn, we will consider two identical spinless bosons as probes, and show that the sign of the interaction affects both the two-particle dynamics and their (quantum) correlations. We will also develop an intuitive picture for this behavior, adding on previous observations [27].

Quantum walks (QWs) describe the dynamics of one or more quantum particles on a lattice [29,30]. They show characteristic quantum features when compared to their classical counterparts—such as ballistic propagation, coherent superposition, and interference of the wave function. These effects make QWs extremely promising for the implementation of quantum algorithms that are faster and more efficient with respect to the protocols traditionally adopted in classical computation [31–33], since they rely on entanglement or other quantum correlations. The potential applications in the field of quantum information inspired a series of recent experimental investigations, which focused on optical networks and quantum optics [34–36], nuclear magnetic resonance, ionic or atomic traps, and quantum-dot arrays (for a recent review, see [37]). In detail, some experimental realizations of

*paolo.bordone@unimore.it

photonic quantum walks (photonic chips) have been achieved [35,38–40], and it was shown that they are capable to act as quantum computing architectures that outperform classical computers in some specific tasks.

In these systems, QWs are typically performed by identical particles, which show very peculiar features: indeed, it has been demonstrated that the indistinguishability of the walkers can build up genuinely quantum correlations even in the absence of interaction between the particles [41,42], as it was observed experimentally in photonic waveguides [34,35,43]. In turn, entanglement among identical particles has raised interest to understand physical phenomena involving highly correlated indistinguishable subsystems. However, despite many efforts [44–62], there are no universally accepted measures for the quantification of this kind of entanglement. Among the different criteria that have been proposed, the so-called *entanglement of particles* [52] is one of the most promising, due to its simple computability, and to the fact that it should be physically measurable in many experimental scenarios [53]. Indeed, it has been recently employed for estimating quantum correlations in spin chains [63,64]—where it is able to detect quantum phase transitions—and in model systems of QWs described by the Hubbard Hamiltonian [28,42,65].

The paper is organized as follows. In Sec . II we introduce the bosonic Hubbard model, whereas in Sec. III we review the theoretical tools to quantify the entanglement between the walkers. Section IV reports the results of our numerical simulations on a chain with $N = 30$ sites, which are then discussed in Sec. V through the help of a simplified semianalytical model (a reduced chain with $N = 4$ sites). Finally, Sec. VI closes the paper with some concluding remarks and Appendix A presents some further discussions about the symmetries of the system, in order to better appreciate the results presented in the body of the paper.

II. INTERACTION MODEL AND THE BAND STRUCTURE

The Bose-Hubbard Hamiltonian describes a collection of spinless bosons propagating on a one-dimensional lattice made of N sites, with periodic boundary conditions ($N + 1 = 1$). The Hamiltonian ($\hbar = 1$) is given by

$$\mathcal{H}_N(J,V) = -J h_N(v),$$
$$h_N(v) = -\sum_{i=1}^{N}(c_{i+1}^{\dagger}c_i + c_i^{\dagger}c_{i+1}) + \frac{v}{2}\sum_{i=1}^{N} n_i(n_i-1), \quad (1)$$

where c_i ($c_i^{\dagger}$) is the operator that destroys (creates) a particle on site i of the chain, J is the hopping amplitude, V is the strength of the interaction among the bosons sharing the same site (attractive for $V < 0$, repulsive for $V > 0$), and $v = V/J$ is the relative strength of the interaction with respect to the hopping energy. In the following we focus on a system with total number of particles $n = 2$. Since J is only a time-dilation factor, giving the characteristic time of the hopping dynamics, we introduce the dimensionless time $\tau = |J|t$. The quantity v is thus the sole parameter changing the physics of the system.

The states of the system can be equally represented in the Fock space and in the symmetrized two-particle Hilbert space, with dimension $N(N+1)/2$ and basis set given by $\{|1,1\rangle_s, |1,2\rangle_s, \ldots, |2,2\rangle_s, \ldots, |N,N\rangle_s\}$, where $|i,j\rangle_s$ ($j \geqslant i$) stands for a symmetrized state in which one particle is localized on site i, and the other on site j. Since the Hubbard Hamiltonian represents the discrete version of the kinetic operator plus a central potential (depending only on the relative distance among the particles), the dynamics can be factorized in the coordinate space of the center of mass $R = \frac{i+j}{2}$ and the relative distance $r = j - i$, so the ansatz for its eigenfunctions becomes

$$\Phi(R,r) = e^{iKR}\varphi(r), \quad (2)$$

and the energy spectrum $E(K) = \omega(K)$ depends on the quasimomentum K, which assumes only discrete values due to the periodic boundary conditions ($K = \frac{2\pi}{N}\nu$, where $\nu = 1, 2, \ldots, N$). The band structure [66] is composed by a *miniband*, hosting N states with energies near V, and a *main subband*, extended approximately between $-4J$ and $+4J$ and hosting the remaining $N(N-1)/2$ states [11,26]. The eigenstates in the miniband are associated with the so-called *bound states*, in which the particles share the same site and show a cowalking dynamics. Conversely, the eigenstates of the main subband, the so-called *scattering states*, have a delocalized wave function [with $\varphi(0) \sim 0$] and show a fermionic antibunching behavior in the high V regime [11]. The striking aspect is that also a repulsive potential may create a bound pair of bosons, as it has been shown experimentally [21]. Indeed, the evolution of particles which are initialized in a bound state is dominated by the states of the miniband, which in the high V regime are well separated in energy from the states of the main subband: therefore, the bound-state particles are forced to remain on the same site while performing their quantum walk.

It has been observed [11,26,67] that the energy spectrum $\mathrm{Spec}[\mathcal{H}_N(J,V)]$ simply changes its sign when we change the sign of V, i.e., $\mathrm{Spec}[\mathcal{H}_N(J,V)] = -\mathrm{Spec}[\mathcal{H}_N(J,-V)]$ (we consider inverse ordering for the two spectra) and, for this reason, it was suggested that the dynamics of the system are the same irrespective of the sign of V [11,21]. However, this symmetry holds only for chains with even N, whereas for chains with odd N, as it is shown in the left panel of Fig. 1 for $N = 5$, the two spectra display some clear discrepancies (mostly in the main subband). If we refer to the two spectra as $\mathrm{Spec}[\mathcal{H}_N(J,\pm V)] = \{\omega_i^{\pm}\}_i$, we may define the deviation D_V

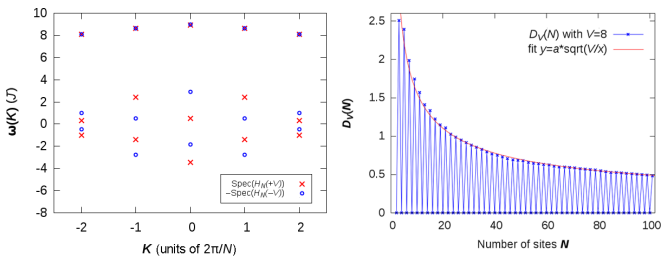

FIG. 1. (Left) Band structure (spectrum) of $\mathcal{H}_N(V)$ and $-\mathcal{H}_N(-V)$ for $V = 8$ and $N = 5$. Energies are given in units of J, wave vectors in units of $2\pi/N$. (Right) Deviation $D_V(N)$ between the spectra of $\mathcal{H}_N(V)$ and $\mathcal{H}_N(-V)$ for $V = 8$ at different values of N. The two spectra are exactly opposite [$D_V(N) = 0$] only for even N. The red line is a phenomenological fit for odd N values.

between them as

$$D_V(N) = \|\mathrm{Spec}[\mathcal{H}_N(V)] + \mathrm{Spec}[\mathcal{H}_N(-V)]\| = \sqrt{\sum_i (\omega_i^+ + \omega_i^-)^2}. \quad (3)$$

The behavior of D_V against N is reported in the right panel of Fig. 1: D_V is always zero for even N, while for odd N it vanishes only in the limit for $N \to \infty$. This suggests that the considered effect is related to differences in periodic boundary conditions, which are less important as soon as N grows. Our observations on the effects of $\mathrm{sgn}(V)$ over dynamics do not depend on N being even or odd. However, in order to avoid the influence of the asymmetry of the band structure, we considered in our simulations only chains with even N. Even in this condition, however, it will be apparent that there are differences in the dynamics when switching from attractive to repulsive interactions (or vice versa).

III. TWO-SITE CORRELATIONS AND ENTANGLEMENT OF PARTICLES

The particle density at each site i of the lattice and the two-particle correlation among sites i and j at a given time t are given by

$$n_i(t) = \langle c_i^\dagger c_i \rangle, \quad (4)$$

$$\Gamma_{i,j}(t) = \langle c_i^\dagger c_j^\dagger c_j c_i \rangle. \quad (5)$$

$\Gamma_{i,j}$ coincides with the diagonal element of the density operator $\rho_{i,j;i,j} = {}_s\langle i,j|\rho|i,j\rangle_s$, whereas for n_i we have $n_i = \sum_i \rho_{i,j;i,j}(1+\delta_{i,j})$. The two-particle correlation is useful to identify behaviors like bunching (or cowalking) and antibunching, which depend both on the initial state $|\Psi(0)\rangle$ and on the strength of the interaction V [11,17]. Here, we will show that it depends on $\mathrm{sgn}(V)$ for some initial states. In particular, for the sake of simplicity we consider the normalized two-particle correlations:

$$\tilde{\Gamma}_{i,j}(t) = \frac{\Gamma_{i,j}(t)}{\max_{\{i,j\}}[\Gamma_{i,j}(t)]}. \quad (6)$$

In order to quantify the entanglement among the walkers, we employ the *entanglement of particles* E_P [52], i.e.,

$$E_P = \sum_{k=0}^{n} P_{k,n-k}\, \mathcal{E}(\rho_{k,n-k}), \quad (7)$$

where, given a bipartition of the sites $A = \{n_{Ai}\}_i$ and $B = \{n_{Bi}\}_i$,

$$\rho_{k,n-k} = \Pi_{k,n-k}\rho\Pi_{k,n-k} \quad (8)$$

is the projection of the system state ρ over the subspace in which A contains exactly k particles and B the remaining $n-k$ ones, whereas $P_{k,n-k} = \mathrm{Tr}[\rho_{k,n-k}]$ is the corresponding probability. For any given bipartition the projectors $\Pi_{k,n-k}$ may be expressed as

$$\Pi_{k,n-k} = \sum_{\Sigma_i n_{Ai}=k} |\{n_{Ai}\}\rangle\langle\{n_{Ai}\}| \otimes \sum_{\Sigma_i n_{Bi}=n-k} |\{n_{Bi}\}\rangle\langle\{n_{Bi}\}|,$$

and satisfying the completeness relation gives $\sum_{k=0}^{n} \Pi_{k,n-k} = \mathbb{I}$. The quantity $\mathcal{E}$ can be any standard measure of bipartite entanglement among the registers individuated by the two partitions. For a two-particle system, the terms with $k = 0$ or $k = 2$ give zero correlations $\mathcal{E} = 0$ and thus Eq. (7) reduces to

$$E_P = P_{1,1}\, \mathcal{E}(\rho_{1,1}). \quad (9)$$

Since we are considering a Hamiltonian system, the states remain pure during all their evolution, and thus we can use the *linear entropy* [47] $\mathcal{E}$,

$$\mathcal{E}(\rho_{AB}) = \frac{N}{N-2}\left(1 - \mathrm{Tr}_A\left[\rho_A^2\right]\right), \quad (10)$$

where $\rho_A = \mathrm{Tr}_B[\rho_{AB}]$ is the reduced density matrix of the subsystem A. Equivalent results may be obtained upon employing the von Neumann entropy or the negativity [68,69].

It is worth noting that E_P depends upon the chosen bipartition of the system modes among Alice and Bob: therefore, different partitions of the system can lead to different values of E_P. Also, it should be mentioned that E_P does not capture all the quantum correlations encoded in the system: indeed, "ideal" cowalking situations, where the particles are strongly correlated, do not give contributions to E_P (since they correspond to $k = 0$ or $k = 2$). On the other hand, those states cannot be exploited to perform any task, since one of the two observers is left with no particle on which she can perform any local operation. E_P thus appears to capture the presence of quantum correlations that represent a resource for quantum information processing.

IV. PROBING THE SIGN BY TWO-PARTICLE QUANTUM WALKS

In this section we describe how the sign of the interaction may be revealed by the features of the walkers' dynamics and by their correlations. As a representative situation, we choose a lattice with $N = 30$ sites. The dynamics of the system is driven either by the Hamiltonian $\mathcal{H}_+ = \mathcal{H}_N(J,V)$ or $\mathcal{H}_- = \mathcal{H}_N(J,-V)$, where $J = 1$. Their spectra $\omega(K)$ (which are symmetrical with respect to $\omega = 0$) are reported in Fig. 2. In

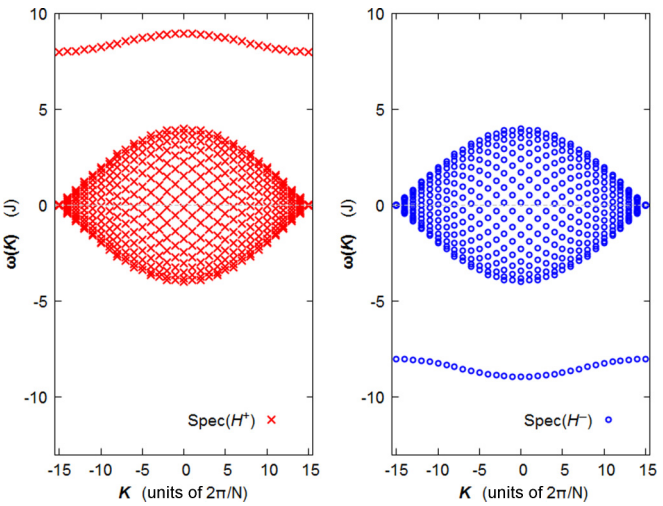

FIG. 2. Band structure $\omega(K)$ of a chain with $N = 30$ sites at $V/J = +8$ (left, red) and $V/J = -8$ (right, blue).

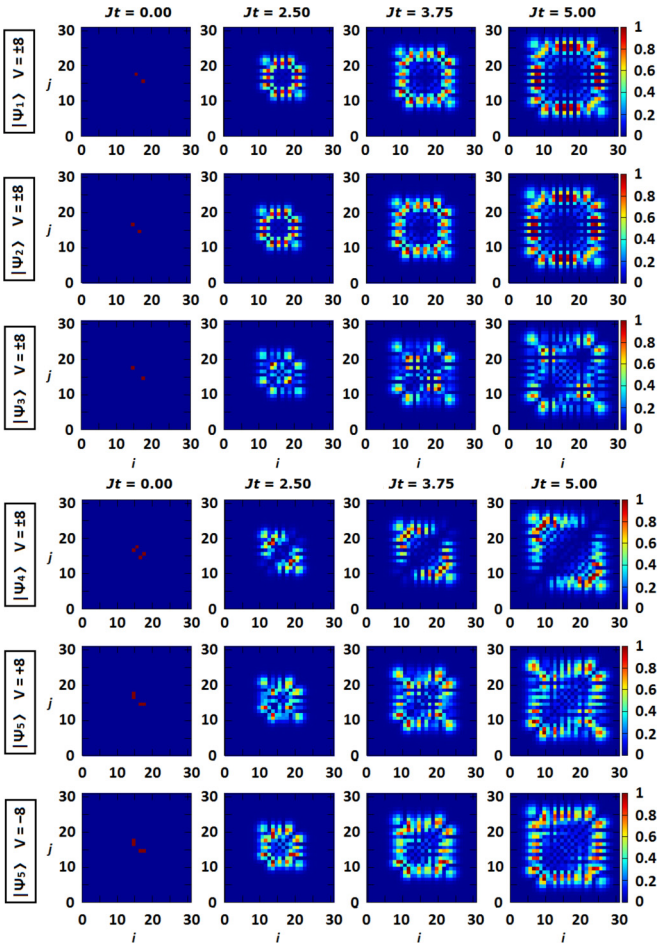

FIG. 3. (Upper panel) Evolution of two-sites correlations $\tilde{\Gamma}_{i,j}$ in states $|\Psi_1\rangle$, $|\Psi_2\rangle$, and $|\Psi_3\rangle$ under $\mathcal{H}_+$ and $\mathcal{H}_-$, with $V = \pm 8$ and $J = 1$. (Lower panel) The same for states $|\Psi_4\rangle$ and $|\Psi_5\rangle$.

studying the dynamics, we limit ourselves to interaction times such that the two particles remain far from the boundaries of the lattice, in order to avoid interference effects due to periodic boundary conditions. Given the initial preparation $\rho(0) = |\Psi(0)\rangle\langle\Psi(0)|$ of the two particles we evaluate the evolved state $\rho(t) = \mathcal{U}_\pm(t)\rho(0)\mathcal{U}_\pm^\dagger(t)$, $\mathcal{U}_\pm(t) = \exp(-i\mathcal{H}_\pm t)$ by numerical diagonalization of the Hamiltonian(s).

As possible initial states $|\Psi(0)\rangle$ we consider the following ones:

$$|\Psi_1\rangle = |15,17\rangle_s, \tag{11}$$

$$|\Psi_2\rangle = |14,16\rangle_s, \tag{12}$$

$$|\Psi_3\rangle = |14,17\rangle_s, \tag{13}$$

$$|\Psi_4\rangle = |14,16\rangle_s + |15,17\rangle_s, \tag{14}$$

$$|\Psi_5\rangle = |14,16\rangle_s + |14,17\rangle_s, \tag{15}$$

which we evolve, alternatively, under the action of $\mathcal{U}_\pm(t)$.

Let us start by looking at the behavior of the correlations $\tilde{\Gamma}_{i,j}$. As it can be seen in the upper panel of Fig. 3, $\tilde{\Gamma}_{i,j}$ for the states $|\Psi_1\rangle$, $|\Psi_2\rangle$, and $|\Psi_3\rangle$ is invariant under the

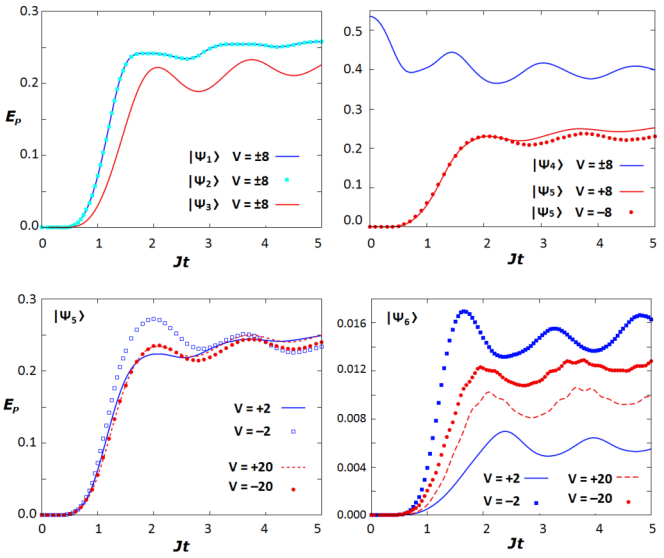

FIG. 4. Time evolution of entanglement of particles under $\mathcal{H}_\pm$. (Upper left) States $|\Psi_1\rangle$, $|\Psi_2\rangle$, and $V = \pm 8$. (Upper right) States $|\Psi_4\rangle$, $|\Psi_5\rangle$ under $\mathcal{H}_\pm$, $V = \pm 8$. (Lower left) State $|\Psi_5\rangle$ and different values of V. (Lower right) State $|\Psi_6\rangle$ and different values of V.

sign exchange of V. The evolution corresponds to the choice $V = \pm 8$; simulations with different values of V lead to the same behavior. Notice that the evolutions of $|\Psi_1\rangle$ and $|\Psi_2\rangle$ are practically identical, except for a rigid shift, and this makes sense since $\mathcal{H}_N$ with periodic boundary conditions commutes with the translation operator $T_l = \Sigma_i |i + l\rangle\langle i|$; therefore, two states that differ only for a rigid shift of $l = 1$ sites ($|\Psi_1\rangle = T_1|\Psi_2\rangle$) should have the same dynamics. The same behavior is found for the entanglement of particles E_P, which is identical both for $\mathcal{H}_+$ and $\mathcal{H}_-$ and is reported in the upper panels of Fig. 4; E_P is initially zero since all states are symmetrized versions of factorizable states. Notice that those initial states are eigenstates of the number operators n_i, i.e., they have an exact number of particles in each site of the lattice. The evolution of these states is invariant when switching from $\mathcal{H}_+$ to $\mathcal{H}_-$ [11]. However, the same consideration does not hold, in general, for superpositions of these states [14,27]: as it can be seen in the lower panel of Fig. 3, the evolution of correlations $\Gamma_{i,j}$ in $|\Psi_4\rangle$ is the same for V and $-V$, whereas the evolution of correlations in $|\Psi_5\rangle$ is appreciably different for attractive and repulsive interactions.

The effects of the interaction sign may be seen also in the dynamics of entanglement of particles (see the upper panels of Fig. 4): E_P for $|\Psi_4\rangle$ is independent from the sign of V, while the entanglement of $|\Psi_5\rangle$ is different for V and $-V$ [notice that $E_P(|\Psi_5\rangle)$ is initially zero since the state is factorizable]. Further analysis shows that this effect depends on the modulus of $|V|$: in Fig. 5, we see that differences in $\tilde{\Gamma}_{i,j}$ for $|\Psi_5\rangle$ are slightly more marked at $V = \pm 2$ than at $V = \pm 20$, and the same behavior is found for entanglement. Indeed, for some states, e.g.,

$$|\Psi_6\rangle = |14,14\rangle_s + |14,17\rangle_s, \tag{16}$$

at low interaction energy $V/J = \pm 2$, E_P may differ by a factor 2, whereas the difference is significantly reduced at higher V

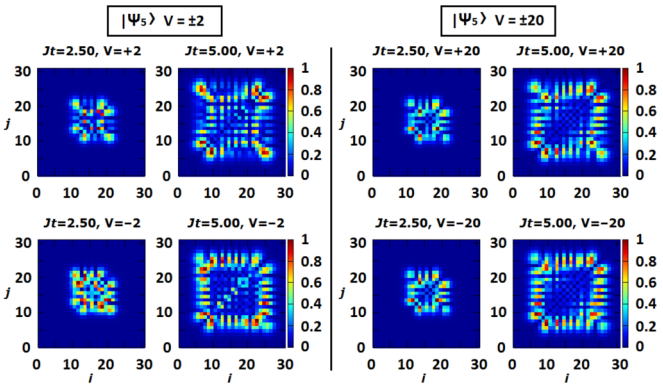

FIG. 5. Evolution of two-sites correlations $\tilde{\Gamma}_{i,j}$ in state $|\Psi_5\rangle$ under $\mathcal{H}_+$ and $\mathcal{H}_-$ for different values of V and for $J = 1$. Differences between evolutions are more apparent at low potential energies (i.e., $V \sim J$).

(see lower panels of Fig. 4). For this particular state, also the differences in correlations $\tilde{\Gamma}_{i,j}$ (here not reported) are more striking at a lower interaction energy (they are 10 times larger at $V = \pm 2$ compared to what may be seen at $V = \pm 20$).

V. DISCUSSION BASED ON AN ANALYTIC TOY MODEL WITH FEW SITES

In order to better understand the behavior of the system, and build an intuitive picture, let us consider an analytic toy model with a chain made of $N = 4$ sites. In the left panel of Fig. 6 we show the band structure of $\mathcal{H}_\pm = \mathcal{H}_4(J, \pm V)$ with $J = 1$ and $V = 8$, whereas the behavior of the eigenvalues of $\mathcal{H}_+$ as a function of V is shown in the central panel. The eigenvalues of $\mathcal{H}_+$ are denoted by ω_i^+ and are reported in Fig. 7, while the eigenvalues of $\mathcal{H}_-$ can be obtained by replacing $\omega_i^- = -\omega_i^+$. However, since the system is invariant under time reversal, any change in the dynamics cannot be related to the simple sign switching of the eigenvalues. The radial part of the eigenfunctions, see Eq. (2), changes sign in some components when switching from $\mathcal{H}_+$ to $\mathcal{H}_-$ [26], while others remain unchanged, suggesting that the different behaviors with attractive or repulsive interactions depend on this feature of the eigenstates.

For what concerns the number eigenstates, due to the translational invariance of the chain, the only states which are physically different are $|1,1\rangle_s$, $|1,2\rangle_s$, and $|1,3\rangle_s$. Each of these states can be decomposed by projection on the eigenstates of the Hamiltonian, leading to

$$|j,k\rangle_s = \sum_i C^{\pm}_{j,k,i} |\Phi^{\pm}_i\rangle. \tag{17}$$

Since the Hamiltonian $\mathcal{H}_\pm$ are real, it is always possible to choose a set of eigenstates $|\Phi^{\pm}_i\rangle$ having real components in the number states basis; therefore, the scalar products

$$C^{\pm}_{j,k,i} = \langle \Phi^{\pm}_i | j,k\rangle_s \tag{18}$$

that we obtain with the projection are real numbers too.

As you can see in Fig. 8, all the projections of states like $|1,1\rangle_s$ and $|1,3\rangle_s$ do not change sign when we switch from $\mathcal{H}_+$ to $\mathcal{H}_-$, while the projections of states like $|1,2\rangle_s$ do change all their signs. This is the reason why superpositions of (translationally) equivalent number eigenstates, like $|\Psi_B\rangle = |1,3\rangle_s + |2,4\rangle_s$, have the same correlations and entanglement independent from the sign of V, while superpositions of nonequivalent number eigenstates, like $|\Xi_B\rangle = |1,4\rangle_s + |2,4\rangle_s$, have a different evolution of their correlations under $\mathcal{H}_+$ and $\mathcal{H}_-$, as it was shown in Ref. [28]. Indeed, the change of sign in V introduces a relative phase between the components of the two number eigenstates, which is different for $\mathcal{H}_+$ and $\mathcal{H}_-$, thus leading to different evolutions of the states.

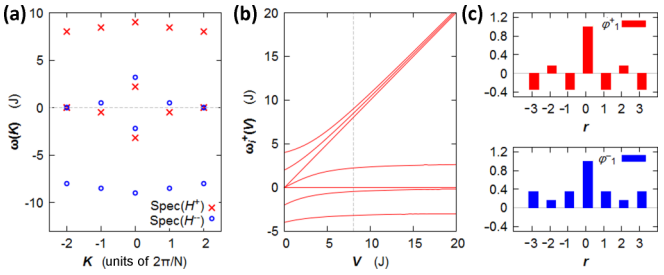

FIG. 6. (a) Band structures for $\mathcal{H}_+$ (red crosses) and $\mathcal{H}_-$ (blue dots) at $V = \pm 8$. The main subband and the miniband are clearly visible, as well as the symmetry of the two spectra. (b) Evolution of the eigenvalues ω_i^+ at increasing V: for high values of the potential energy, there is a clear separation between the miniband (which becomes almost flat) and the main subband, while at low V the two subbands are entwined. The gray vertical dashed line indicates $V = 8$ (a). (c) Radial wave function for the first eigenstate of $\mathcal{H}_+$ (upper, red) and $\mathcal{H}_-$(lower, blue).

$$\mathcal{U}(t)(|1,3\rangle_s + |2,4\rangle_s) = \begin{cases} \sum_i (C^+_{1,3,i} + C^+_{2,4,i})|\Phi^+_i(t)\rangle & V > 0, \\ \sum_i (C^+_{1,3,i} + C^+_{2,4,i})|\Phi^-_i(t)\rangle & V < 0, \end{cases} \tag{19}$$

$$\mathcal{U}(t)(|1,4\rangle_s + |2,4\rangle_s) = \begin{cases} \sum_i (C^+_{1,4,i} + C^+_{2,4,i})|\Phi^+_i(t)\rangle & V > 0, \\ \sum_i (-C^+_{1,4,i} + C^+_{2,4,i})|\Phi^-_i(t)\rangle & V < 0, \end{cases} \tag{20}$$

		Eigenvalue	Degen.
Miniband	ω_1^+	$\frac{V}{3} + \frac{48J^2+V^2}{9\gamma} + \gamma$	1
	$\omega_{2,3}^+$	$\frac{V+\sqrt{16J^2+V^2}}{2}$	2
	ω_4^+	V	1
Main subband	ω_5^+	$V + \omega_1^+(J,-V) - \omega_1^+(J,V) = \frac{V}{3} + \left(\frac{48J^2+V^2}{9\gamma\gamma'} - 1\right)(\gamma - \gamma')$	1
	$\omega_{6,7}^+$	$\frac{V-\sqrt{16J^2+V^2}}{2}$	2
	$\omega_{8,9}^+$	0	2
	ω_{10}^+	$-\omega_1^+(J,-V) = \frac{V}{3} - \frac{48J^2+V^2}{9\gamma'} - \gamma'$	1

$$\gamma(J,V) = \left(\sqrt{\left(\frac{4J^2V}{3} - \frac{V^3}{27}\right)^2 - \left(\frac{16J^2}{3} + \frac{V^2}{9}\right)^3} - \frac{4J^2V}{3} + \frac{V^3}{27}\right)^{\frac{1}{3}} \qquad \gamma' = \gamma(J,-V)$$

FIG. 7. Eigenvalues of $\mathcal{H}_+$ with relative multiplicity (degeneracy), ordered by decreasing energy.

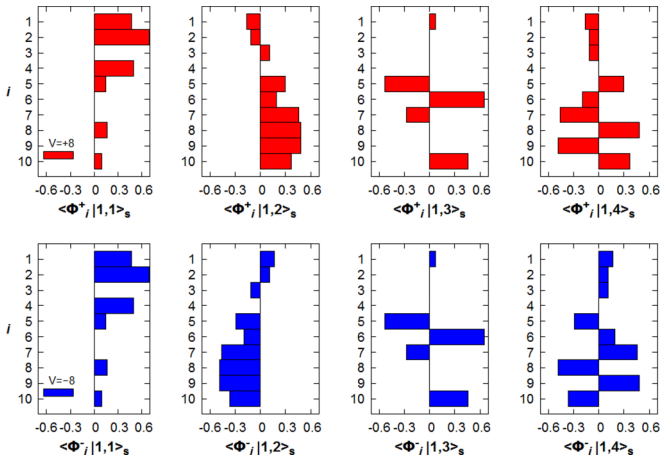

FIG. 8. Projections of number states $|1,1\rangle_s$, $|1,2\rangle_s$, $|1,3\rangle_s$, and $|1,4\rangle_s$ over the eigenstates of $\mathcal{H}_+$ (first row, red) and $\mathcal{H}_-$ (second row, blue) for a potential energy of $|V| = 8$. Notice that, as expected, $|1,4\rangle_s$ behaves like $|1,2\rangle_s$, and their projections are also identical in modulus (since the two states are translationally equivalent).

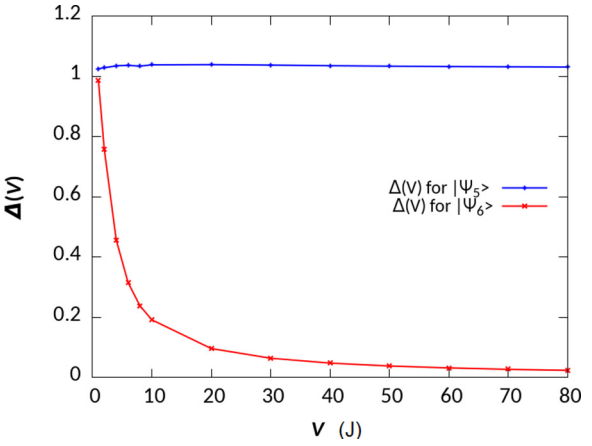

FIG. 9. Total difference $\Delta(V)$ among the projections of a state $|\Psi\rangle$ over the eigenstates of $\mathcal{H}$ for positive and negative V.

It should be emphasized that the coefficients $C^{\pm}_{j,k,i}$ change sign when we change the sign of V; therefore, we cannot observe this effect directly when we study a single number eigenstate [e.g., by setting $|\Psi(0)\rangle = |1,3\rangle_s$], because the squared modulus of the projections does not depend on $\mathrm{sgn}(C^{\pm}_{j,k,i})$. Only superpositions of number eigenstates keep trace of the sign of the interaction [14,27]. This is perhaps the reason why many previous works in the literature did not observe this dependence. Indeed, going back to our calculations on the 1D chain with $N = 30$, we notice that states like $|\Psi_1\rangle$ and $|\Psi_2\rangle$ are of the same kind, i.e., second nearest neighbors like $|i,i+2\rangle_s$ (this is the reason why they show the same evolution of two-site correlations—except for a rigid translation), while the state $|\Psi_3\rangle$ is a third nearest-neighbor state, like $|i,i+3\rangle_s$. This is the reason why $|\Psi_1\rangle$ and $|\Psi_2\rangle$ have equal projections on the eigenstates of $\mathcal{H}_\pm$, whereas the projections of $|\Psi_3\rangle$ are different. Therefore, the linear combination of $|\Psi_1\rangle$ and $|\Psi_2\rangle$ is invariant under the exchange of $\mathrm{sgn}(V)$, while the linear combination of $|\Psi_2\rangle$ and $|\Psi_3\rangle$ is not (some projections exchange sign for a state but not for the other).

Concerning the behavior of a state like $|\Psi_6\rangle$, the effect of switching the sign of V is more visible at low potential energy, since for $V \sim J$ the main subband and the miniband are strongly mixed, such that each number eigenstate has a projection over all the eigenvectors of $\mathcal{H}_\pm$, and states with different nature have therefore very different superpositions under $\mathcal{H}_+$ and $\mathcal{H}_-$. On the contrary, for large values of V/J the entanglement is not so much different, due to the strong separation between the subband and the miniband (see Fig. 6). Indeed, this separation implies that the projections of the bound state $|14,14\rangle_s$ are almost completely contained in the miniband, while the ones of the scattering state $|14,17\rangle_s$ are mainly in the main subband. Therefore, the expressions $C^{\pm}_{14,14,i} + C^{\pm}_{14,17,i}$ do not change significantly their (absolute) values when switching from $\mathcal{H}_+$ to $\mathcal{H}_-$ since, for each i, only one coefficient in the sum is significantly different from zero. Note that this behavior can be generalized to a lattice with an arbitrary number of sites, provided that such number is even, as shown in Appendix B.

This phenomenon may be better illustrated upon introducing a quantity $\Delta(V)$ that quantifies the difference between the projections of a state $|\Psi\rangle$ over the eigenstates of $\mathcal{H}_+$ and $\mathcal{H}_-$ as a function of V. To this aim we first consider the sum of the squared modulus of all the projections over the eigenstates with degenerate energies, i.e., $P^{\pm}(\omega) = \sum_{\omega_i=\omega} |\langle\Phi^{\pm}_i|\Psi\rangle|^2$. Then, for each projection $P(\omega)$ on a degenerate energy subspace, we evaluate the absolute difference between P at positive and negative V:

$$\Delta_\omega(V) = |P^+(\omega) - P^-(\omega)|^2, \tag{21}$$

in order to determine how much the projections of $|\Psi\rangle$ change when switching from $|\Phi^+_i\rangle$ to $|\Phi^-_i\rangle$. Finally, we sum over the different energies of the Hamiltonian, and we get the desired figure of merit:

$$\Delta(V) = \sum_\omega \Delta_\omega(V). \tag{22}$$

As we can observe in Fig. 9, the quantity $\Delta(V)$ goes to zero for the state $|\Psi_6\rangle$, due to the progressive separation between the scattering subband and the miniband at increasing values of V/J. In turn, this is the reason for which the changes in entanglement and in correlations (when switching from positive to negative potentials) are more relevant at low interaction energies. A similar line of reasoning does not hold for $|\Psi_5\rangle$, which is composed by the scattering states $|14,16\rangle_s$ and $|14,17\rangle_s$, both belonging to the main subband: as we can see from Fig. 9, the differences in the projections $\Delta(V)$ for $|\Psi_5\rangle$ are nearly constant when we increase V. Indeed, we do not observe a significant change either in entanglement or in the correlation maps at increasing V, as we see in Figs. 4 and 5.

As a final remark, we recall that the band structure for a chain of N sites is composed by a miniband, hosting N states with energies near V, and a main subband, extended approximately between $-4J$ and $+4J$, hosting the remaining states. The eigenstates of the miniband are associated with the so-called bound states, in which the two bosons share the same site and show a cowalking (bunching) dynamics, independently on the sign of the potential. Conversely, the eigenstates of the main subband, the so-called scattering

states, have a delocalized wave function and show a fermionic antibunching behavior in the high V regime (even for attractive potentials). If we initialize our particles in an interacting state like $|1,1\rangle$, that state has projections mainly over the bound eigenstates of the Hamiltonian. Therefore, its evolution is dominated by the states of the miniband, which in the high V regime are well separated in energy from the states of the main subband. Conversely, particles initialized in a noninteracting state like $|1,2\rangle$ have a dynamics which is dominated by the scattering states of the main subband, and therefore they show an antibunching behavior at high V. At low potentials, all states have nonzero projections over both the miniband and the scattering subband, so we observe a dynamics with a mixed character, while at high V the number state projections in the two subbands, and consequently the two kinds of dynamics, are well distinguished.

VI. CONCLUSIONS

In this paper we have shown that in the Bose-Hubbard model both two-site correlations and entanglement of particles are differently affected by on-site attractive and repulsive interactions. These differences are more significant for low values of the interaction V, i.e., of the order of the hopping amplitude J, thus making this regime achievable using current technologies [21,22]. This behavior arises from the fact that the projections of some localized number states on the eigenfunctions of the Hubbard model may change sign when we change the sign of V. Therefore, the effect of $\mathrm{sgn}(V)$ may be observed by observing the evolution of linear combinations of number states. This also explains why these features have not been pointed out and observed before, since most of the present literature is mainly focused on the study of single number states.

The quantitative dependence of correlations on the sign of V may be relevant, up to a factor 2, as we have seen for entanglement. This phenomenon also provides a further degree of freedom for manipulating the correlations in a quantum walk, and may be exploited to perform specific tasks in quantum information processing.

Besides revealing additional features of the Hubbard model, and providing a probing technique, our results pave the way to further research aimed at investigating whether this behavior may be observed in some extensions of the Hubbard model—e.g., the Fermi-Hubbard model for spinless fermions (the so-called fermion-polaron model [66])—or if it is an exclusive feature of bosonic Hubbard (or sermonic) models. Indeed, some recent works [70] have shown a breaking of the symmetry $\pm V$ for long-range hopping in hard-core bosons. Besides, it seems worth exploring the signatures of long-range hopping and interactions (i.e., extended to first- and second-nearest-neighboring sites) on the dynamics and the entanglement of both bosonic and fermionic particles.

ACKNOWLEDGMENTS

This work has been supported by UNIMORE through FAR2014 and by EU through the collaborative H2020 project QuProCS (Grant Agreement No. 641277). The authors thank Ilaria Siloi for fruitful discussions. P.B. and M.G.A.P. thank Gruppo Nazionale per la Fisica Matematica (GNFM-INdAM).

APPENDIX A: INVARIANCE UNDER BOOST AND TIME-REVERSAL TRANSFORMATIONS

In this section we want to further discuss the symmetries of the Hamiltonians $\mathcal{H}_\pm = \mathcal{H}_N(J, \pm V)$ [14,27] in order to better appreciate the results presented in the body of the paper. In particular, we want to emphasize that the expectation value of an operator O on state $|\psi(t)\rangle_\pm = \exp(-iH_\pm t)|\psi_0\rangle$ is independent from the sign of V if both the initial state $|\psi_0\rangle$ and O are invariant under both *boost transformation* and *time-reversal transformation*. In order to better illustrate these features we will go through the explicit proof of the invariance.

The idempotent Hermitian *boost operator*, $B = B^\dagger$, $B^2 = 1$, is defined by its action in k space: $Ba_k^\dagger B = a_{k+\pi}^\dagger$, whereas in the x space we have $Bc_jB = e^{-\mathrm{i}\pi j}c_j$. As a consequence, we may write

$$B\mathcal{H}_\pm B = -\mathcal{H}_\mp. \tag{A1}$$

B being a unitary operator any eigenstate of B is actually invariant under the action of B. The same discussion does not hold, of course, for combinations of eigenstates belonging to different eigenvalues. The *time-reversal operator* is the antiunitary operator Θ defined by $\Theta e^{-iH_\pm t}\Theta^\dagger = e^{+iH_\pm t}$ and $\Theta|\psi_0\rangle = |\psi_0^*\rangle$ and which may be written as $\Theta = KU$, where U is a unitary operator and K is the complex-conjugation operator. An operator is said to have a well-defined symmetry under time reversal if it is even (invariant) or odd, $\Theta O\Theta^\dagger = \pm O$.

Let us consider now the expectation value of O under $\mathcal{H}_+$, i.e., $\langle O(t)\rangle_+ = \langle\psi_0|\exp(+i\mathcal{H}_+t)O\exp(-i\mathcal{H}_+t)|\psi_0\rangle$. Under the hypothesis that both O and $|\psi_0\rangle$ are invariant under B we have

$$\begin{aligned}\langle O(t)\rangle_+ &= \langle\psi_0|\exp(-i\mathcal{H}_-t)O\exp(+i\mathcal{H}_-t)|\psi_0\rangle \\ &= \langle O(-t)\rangle_-.\end{aligned} \tag{A2}$$

If we also consider the invariance under time reversal of both O and $|\psi_0\rangle$, we get finally

$$\begin{aligned}\langle O(t)\rangle_+ &= \langle O(-t)\rangle_- \\ &= \langle\psi_0|\exp(+i\mathcal{H}_-t)O\exp(-i\mathcal{H}_-t)|\psi_0\rangle \\ &= \langle O(t)\rangle_-,\end{aligned} \tag{A3}$$

so that the switching of the sign of the potential produces no effect on the expectation value of O. Overall, we may conclude that, in general, if the state and the observable are invariant under boost transformation, when we switch the sign of the potential V we actually reverse the direction of time: some observables, like the entanglement, are not affected by this operation, while others are. In particular, if we look at the correlation maps, changing the direction of time is equal to changing sign to all the velocity components of the wave functions, so that left and right directions are reversed (i.e., the correlation maps become specular). However, this phenomenon is not observable if the velocity composition is symmetrical (i.e., it determines a symmetrical expansion on the map), but in the opposite case it can be spotted. This is

particularly apparent for states like $|\psi\rangle = |14,16\rangle_s + |15,17\rangle_s$, where entanglement and correlation maps are identical (both states have the same eigenvalue with respect to B). On the other hand, if we add a complex relative phase, i.e., $|\psi\rangle = |14,16\rangle_s + i|15,17\rangle_s$, we break the time-reversal invariance and we make the velocity composition asymmetrical. In this case, the entanglement does not change its dynamics, but the correlation maps are reversed with respect to their antidiagonal.

APPENDIX B: MAPPING $\mathcal{H}_+$ INTO $\mathcal{H}_-$

In this section we generalize the result given in Sec. V for the case of a lattice with an even number of sites. In fact, in this case, it is possible to identify a unitary transformation that maps $\mathcal{H}_+$ into $\mathcal{H}_-$. It is possible to realize such a unitary transformation by noting that the sign change of c_i at every other site, $c_i \to (-1)^i c_i$, changes the sign of the hopping term, but leaves the interaction term unchanged. This explains not only the relation between the spectra, but also the relation between the eigenstates of $\mathcal{H}_+$ and $\mathcal{H}_-$. As an example, let us suppose that a two-particle eigenstate of $\mathcal{H}_+$, corresponding, say, to the eigenvalue ε is given by

$$|\Psi_+\rangle = \sum_{i,j} \alpha_{i,j} |i,j\rangle_s, \tag{B1}$$

where $|i,j\rangle_s = c_i^\dagger c_j^\dagger |0\rangle$, with $|0\rangle$ being the vacuum state. Then the above unitary transformation implies that the state

$$|\Psi_-\rangle = \sum_{i,j} (-1)^{i+j} \alpha_{i,j} |i,j\rangle_s \tag{B2}$$

is an eigenstate of $\mathcal{H}_-$ with eigenvalue $-\varepsilon$. Therefore, comparing the eigenstates of $\mathcal{H}_+$ with the ones of $\mathcal{H}_-$, only the components with $i + j$ odd change their sign. This explains why the dynamics of quantum correlations is sensitive to the sign of V when the initial state is a superposition of states with different parity.

[1] F. H. Essler, H. Frahm, F. Göhmann, A. Klümper, and V. E. Korepin, *The One-dimensional Hubbard Model* (Cambridge University Press, Cambridge, UK, 2005).

[2] A. Montorsi, *The Hubbard Model: A Reprint Volume* (World Scientific, Singapore, 1992).

[3] E. H. Lieb and F. Wu, Physica A **321**, 1 (2003).

[4] L. Amico, R. Fazio, A. Osterloh, and V. Vedral, Rev. Mod. Phys. **80**, 517 (2008).

[5] P. M. Preiss, R. Ma, M. E. Tai, A. Lukin, M. Rispoli, P. Zupancic, Y. Lahini, R. Islam, and M. Greiner, Science **347**, 1229 (2015).

[6] L.-M. Duan, E. Demler, and M. D. Lukin, Phys. Rev. Lett. **91**, 090402 (2003).

[7] T. Fukuhara, P. Schauß, M. Endres, S. Hild, M. Cheneau, I. Bloch, and C. Gross, Nature (London) **502**, 76 (2013).

[8] D. Jaksch and P. Zoller, Ann. Phys. (N.Y.) **315**, 52 (2005), special issue.

[9] T. Fukuhara, A. Kantian, M. Endres, M. Cheneau, P. Schauß, S. Hild, D. Bellem, U. Schollwöck, T. Giamarchi, C. Gross *et al.*, Nat. Phys. **9**, 235 (2013).

[10] H. J. Schulz, Phys. Rev. Lett. **64**, 2831 (1990).

[11] Y. Lahini, M. Verbin, S. D. Huber, Y. Bromberg, R. Pugatch, and Y. Silberberg, Phys. Rev. A **86**, 011603 (2012).

[12] Y. Bromberg, Y. Lahini, E. Small, and Y. Silberberg, Nat. Photon. **4**, 721 (2010).

[13] F. Lederer, G. I. Stegeman, D. N. Christodoulides, G. Assanto, M. Segev, and Y. Silberberg, Phys. Rep. **463**, 1 (2008).

[14] C. Lee, A. Rai, C. Noh, and D. G. Angelakis, Phys. Rev. A **89**, 023823 (2014).

[15] S. Longhi, J. Phys. B **44**, 051001 (2011).

[16] T. Matsubara and H. Matsuda, Prog. Theor. Phys. **16**, 569 (1956).

[17] X. Qin, Y. Ke, X. Guan, Z. Li, N. Andrei, and C. Lee, Phys. Rev. A **90**, 062301 (2014).

[18] L. Wang, L. Wang, and Y. Zhang, Phys. Rev. A **90**, 063618 (2014).

[19] L. Wang, N. Liu, S. Chen, and Y. Zhang, Phys. Rev. A **92**, 053606 (2015).

[20] J. Hecker Denschlag and A. J. Daley, in *Proceedings of the International School of Physics "Enrico Fermi"* (IOS Press Ebooks, Amsterdam, 2007), Vol. 164.

[21] K. Winkler, G. Thalhammer, F. Lang, R. Grimm, J. H. Denschlag, A. Daley, A. Kantian, H. Büchler, and P. Zoller, Nature (London) **441**, 853 (2006).

[22] L. Wang, Y. Hao, and S. Chen, Phys. Rev. A **81**, 063637 (2010).

[23] S. Fölling, S. Trotzky, P. Cheinet, M. Feld, R. Saers, A. Widera, T. Müller, and I. Bloch, Nature (London) **448**, 1029 (2007).

[24] R. Piil and K. Mølmer, Phys. Rev. A **76**, 023607 (2007).

[25] L. Wang, Y. Hao, and S. Chen, Eur. Phys. J. D **48**, 229 (2008).

[26] M. Valiente and D. Petrosyan, J. Phys. B **41**, 161002 (2008).

[27] U. Schneider, L. Hackermüller, J. P. Ronzheimer, S. Will, S. Braun, T. Best, I. Bloch, E. Demler, S. Mandt, D. Rasch *et al.*, Nat. Phys. **8**, 213 (2012).

[28] A. Beggi, F. Buscemi, and P. Bordone, Quantum Inf. Process. **15**, 3711 (2016).

[29] J. Kempe, Contemp. Phys. **44**, 307 (2003).

[30] S. Venegas-Andraca, Quantum Inf. Process. **11**, 1015 (2012).

[31] A. Ambainis, Int. J. Quantum Inf. **01**, 507 (2003).

[32] R. Portugal, *Quantum Walks and Search Algorithms* (Springer Science & Business Media, New York, 2013).

[33] S. E. Venegas-Andraca, Synth. Lect. Quantum Comput. **1**, 1 (2008).

[34] Y. Bromberg, Y. Lahini, R. Morandotti, and Y. Silberberg, Phys. Rev. Lett. **102**, 253904 (2009).

[35] A. Peruzzo, M. Lobino, J. C. F. Matthews, N. Matsuda, A. Politi, K. Poulios, X.-Q. Zhou, Y. Lahini, N. Ismail, K. Wrhoff *et al.*, Science **329**, 1500 (2010).

[36] A. Rai, G. S. Agarwal, and J. H. H. Perk, Phys. Rev. A **78**, 042304 (2008).

[37] J. Wang and K. Manouchehri, *Physical Implementation of Quantum Walks* (Springer, New York, 2013).

[38] M. A. Broome, A. Fedrizzi, S. Rahimi-Keshari, J. Dove, S. Aaronson, T. C. Ralph, and A. G. White, Science **339**, 794 (2013).

[39] J. B. Spring, B. J. Metcalf, P. C. Humphreys, W. S. Kolthammer, X.-M. Jin, M. Barbieri, A. Datta, N. Thomas-Peter, N. K. Langford, D. Kundys *et al.*, Science **339**, 798 (2013).
[40] M. Tillmann, B. Dakić, R. Heilmann, S. Nolte, A. Szameit, and P. Walther, Nat. Photon. **7**, 540 (2013).
[41] J. D. Franson, Science **339**, 767 (2013).
[42] C. Benedetti, F. Buscemi, and P. Bordone, Phys. Rev. A **85**, 042314 (2012).
[43] K. Mayer, M. C. Tichy, F. Mintert, T. Konrad, and A. Buchleitner, Phys. Rev. A **83**, 062307 (2011).
[44] J. Schliemann, J. I. Cirac, M. Kuś, M. Lewenstein, and D. Loss, Phys. Rev. A **64**, 022303 (2001).
[45] K. Eckert, J. Schliemann, D. Bru, and M. Lewenstein, Ann. Phys. (N.Y.) **299**, 88 (2002).
[46] F. Buscemi, P. Bordone, and A. Bertoni, Phys. Rev. A **73**, 052312 (2006).
[47] F. Buscemi, P. Bordone, and A. Bertoni, Phys. Rev. A **75**, 032301 (2007).
[48] P. Zanardi, Phys. Rev. A **65**, 042101 (2002).
[49] G. C. Ghirardi, L. Marinatto, and T. Weber, J. Stat. Phys. **108**, 49 (2002).
[50] G. C. Ghirardi and L. Marinatto, Phys. Rev. A **70**, 012109 (2004).
[51] F. Benatti, R. Floreanini, and K. Titimbo, Open Syst. Inf. Dyn. **21**, 1440003 (2014).
[52] H. M. Wiseman and J. A. Vaccaro, Phys. Rev. Lett. **91**, 097902 (2003).
[53] M. R. Dowling, A. C. Doherty, and H. M. Wiseman, Phys. Rev. A **73**, 052323 (2006).
[54] T. Sasaki, T. Ichikawa, and I. Tsutsui, Phys. Rev. A **83**, 012113 (2011).
[55] F. Iemini, T. Maciel, T. Debarba, and R. Vianna, Quantum Inf. Process. **12**, 733 (2013).
[56] F. Iemini and R. O. Vianna, Phys. Rev. A **87**, 022327 (2013).
[57] F. Iemini, T. Debarba, and R. O. Vianna, Phys. Rev. A **89**, 032324 (2014).
[58] A. Reusch, J. Sperling, and W. Vogel, Phys. Rev. A **91**, 042324 (2015).
[59] P. Zanardi, D. A. Lidar, and S. Lloyd, Phys. Rev. Lett. **92**, 060402 (2004).
[60] H. Barnum, E. Knill, G. Ortiz, R. Somma, and L. Viola, Phys. Rev. Lett. **92**, 107902 (2004).
[61] F. Benatti, R. Floreanini, and U. Marzolino, Phys. Rev. A **85**, 042329 (2012).
[62] F. Benatti, R. Floreanini, and U. Marzolino, Phys. Rev. A **89**, 032326 (2014).
[63] L. Mazza, D. Rossini, R. Fazio, and M. Endres, New J. Phys. **17**, 013015 (2015).
[64] F. Iemini, T. O. Maciel, and R. O. Vianna, Phys. Rev. B **92**, 075423 (2015).
[65] F. Buscemi and P. Bordone, Phys. Rev. A **84**, 022303 (2011).
[66] A. Scott, J. Eilbeck, and H. Gilhøj, Physica D **78**, 194 (1994).
[67] M. Valiente, Phys. Rev. A **81**, 042102 (2010).
[68] D. Girolami and G. Adesso, Phys. Rev. A **84**, 052110 (2011).
[69] S. Lee, D. P. Chi, S. D. Oh, and J. Kim, Phys. Rev. A **68**, 062304 (2003).
[70] T. Chattaraj and R. V. Krems, Phys. Rev. A **94**, 023601 (2016).